10
Drift chambers

A drift chamber is a particle tracking device that uses the drift time of ionization electrons in a gas to measure the spatial position of an ionizing particle [1 – 3]. Drift chambers can achieve spatial resolutions an order of magnitude smaller than MWPCs. A typical timing measurement accuracy of 2 ns and a drift velocity of 4 cm/μs corresponds to a theoretical spatial accuracy of 80 μm. Drift chambers have found wide acceptance as charged particle tracking detectors in spectrometer systems. When covering large solid angles, drift chambers provide resolution equal to MWPCs at a much lower cost.

A typical drift chamber arrangement is shown in Fig. 10.1. A region of approximately uniform field is set up between the anode and cathode wires. A charged particle traversing the chamber liberates electrons that drift toward the anodes. The passage of the particle also generates a fast pulse in the scintillation counter that can be used to define a reference time t_0. The electrons drift for a time Δt, after which they are collected at the anode, thereby providing a signal that a particle has passed. The position where the particle traversed the chamber is then given by

$$x = \int_{t_0}^{t_0+\Delta t} w(t)\, dt \tag{10.1}$$

where $w(t)$ is the drift velocity.

10.1 Properties of drift chamber gases

The passage of ionizing radiation through the gas in a drift chamber cell leaves behind a trail of electrons and positive ions. In order to use the electron arrival times to accurately locate the position in the chamber that was traversed by the incoming particle, we must have an

https://doi.org/10.1017/9781009290098.011 Published online by Cambridge University Press

accurate knowledge of the drift velocity of the electrons in the gas. The liberated electrons have inelastic collisions with the surrounding gas molecules and quickly establish a Maxwellian distribution of velocities. The most probable random (or thermal) electron energy at room temperature is ~ 0.04 eV. When an electric field $\mathscr{E}$ is applied, the component of the drift velocity w parallel to the field is [4, 5]

$$w_{\parallel} = \frac{2}{3}\frac{e\mathscr{E}}{m}\left\langle\frac{\lambda}{v}\right\rangle + \frac{1}{3}\frac{e\mathscr{E}}{m}\left\langle\frac{d\lambda}{dv}\right\rangle \tag{10.2}$$

where e and m are the charge and mass of the electron and $\lambda(v)$ is the mean free path for an electron with random velocity v in the drift chamber gas. The averages must be performed over the distribution of electron random velocities. The variation of λ with v is often ignored when estimating gas properties. Note that $\langle\lambda/v\rangle$ is the mean time between collisions. Some measurements of drift velocities in pure gases are given in Table 10.1.

If a magnetic field B perpendicular to $\mathscr{E}$ is also present, the drift velocity will have a component along the direction $\mathscr{E} \times \mathbf{B}$ given by

$$w_{\perp} = \left(1 + \frac{e^2B^2\lambda^2}{m^2v^2}\right)^{-1}\left(\frac{1}{3}\frac{e\mathscr{E}}{m}\omega_{\mathrm{L}}\left\langle\frac{\lambda^2}{v^2}\right\rangle + \frac{2}{3}\frac{e\mathscr{E}}{m}\omega_{\mathrm{L}}\left\langle\frac{\lambda}{v}\frac{d\lambda}{dv}\right\rangle\right) \tag{10.3}$$

Figure 10.1 Principle of operation of a drift chamber.

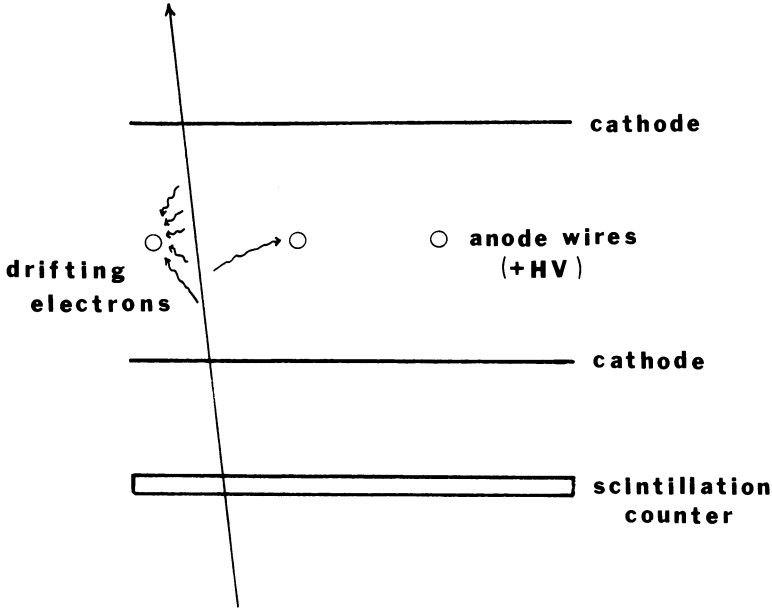

https://doi.org/10.1017/9781009290098.011 Published online by Cambridge University Press

where

$$\omega_L = eB/m \tag{10.4}$$

is the Larmor precession frequency. The net drift angle with respect to $\mathscr{E}$ in this case would be

$$\tan \alpha = w_\perp / w_\parallel \tag{10.5}$$

Figure 10.2 shows measurements of the drift angle as a function of $\mathscr{E}$ and B. Besides electric and magnetic fields, other factors that can influence the drift velocity include the temperature and pressure of the gas and the addition of "impurity" gases. Note that the drift velocity is a function of $\mathscr{E}/P$, where P is the gas pressure.

A second important property of a drift chamber gas is the diffusion coefficient for electrons traveling through the gas. The amount of diffusion that occurs limits the spatial resolution obtainable with the chamber. According to classical kinetic theory, the electron cloud will diffuse, as it drifts along with a diffusion coefficient D, given by

$$D = \tfrac{1}{3} \langle \lambda v \rangle \tag{10.6}$$

Table 10.1. *Drift velocities of pure gases, STP (cm/μs)*

	$\mathscr{E}$ (kV/cm)		
Gas	1	2	3
CH_4	10.4	8.5	7.1
C_2H_6	5.2	5.5	5.5
C_3H_8	4.0	4.7	4.9
Iso-C_4H_{10}	3.3	5.1	
C_2H_4	4.8	5.1	4.8
He	1.0	1.6	2.3
Ar	0.4	0.7	1.1
Ar (liquid)	0.2	0.3	0.3
Xe	0.2	0.4	0.6
H_2	1.1	1.8	2.0
N_2	0.9	1.4	2.0
O_2	2.4	3.1	3.8
CO_2	0.7	1.5	2.6
$CH_2(OCH_3)_2$	0.7	1.5	2.1

Source: A. Peisert and F. Sauli, CERN Report 84-08, 1984; B. Jean-Marie, V. Lepeltier, and D. L'Hote, Nuc. Instr. Meth. 159: 213, 1979; F. Sauli, CERN Report 77-09, 1977.

After drifting a distance x, each component of the electron's position becomes dispersed by an amount

$$\sigma_x = \sqrt{\frac{2Dx}{w}} \tag{10.7}$$

Note, however, that the diffusion coefficient need not be isotropic.

Simple estimates for the magnitudes of the transport coefficients have been given by Palladino and Sadoulet [4] using conservation of energy arguments. The electron cloud tends to be accelerated by the electric field. On the other hand, collisions between the electrons and the gas atoms occur with a mean time between collisions of v/λ. After a time $\sim 10^{-11}$ sec the electron cloud reaches equilibrium with the gas and travels with an approximately constant drift velocity. If $\Gamma(E)$ is the mean fractional energy loss per collision, then the energy gained per unit time from the electric field must equal the energy lost per unit time in atomic collisions, or

$$e\mathscr{E}w_{\parallel} = \left\langle \Gamma E \frac{v}{\lambda} \right\rangle$$

If we assume λ is independent of v and that the energy distribution is narrow, then

$$e\mathscr{E}w_{\parallel} \simeq \tfrac{1}{2} mv^2 \Gamma \frac{v}{\lambda}$$

Figure 10.2 Drift angle as a function of electric and magnetic fields. (U. Becker, M. Capell, D. Osborne, and C. Ye, Nuc. Instr. Meth. 205: 137, 1983.)

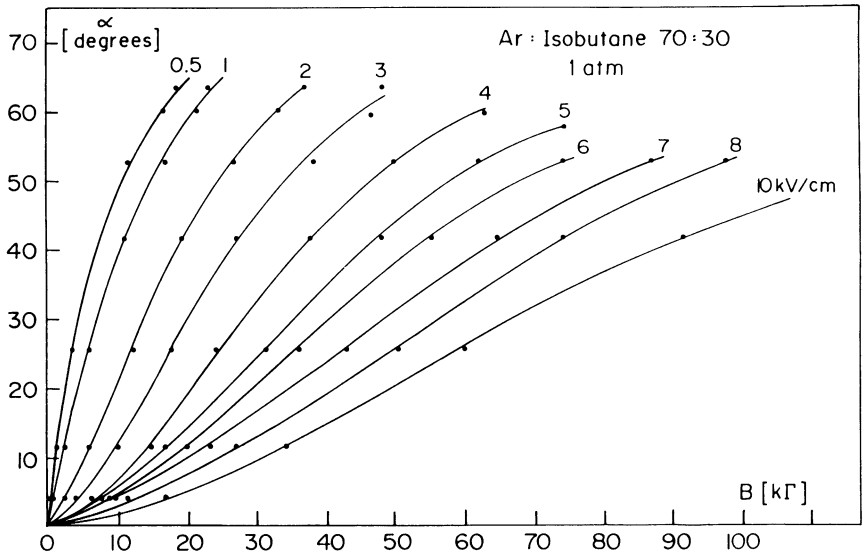

https://doi.org/10.1017/9781009290098.011 Published online by Cambridge University Press

Substituting $w_\parallel$ from Eq. 10.2, we obtain the following expression for v:

$$v = \left[\frac{2e\mathscr{E}\lambda}{(3\Gamma)^{1/2}m}\right]^{1/2} \tag{10.8}$$

It is convenient to use Eq. 10.8 to express the various transport coefficients in terms of λ and Γ. Thus, we find that the components of the drift velocity are

$$w_\parallel = \left(\frac{2}{3}\frac{e\mathscr{E}\lambda}{m}\left(\frac{\Gamma}{3}\right)^{1/2}\right)^{1/2} \tag{10.9}$$

$$w_\perp = \frac{eB\lambda}{6m}(3\Gamma)^{1/2} \tag{10.10}$$

The mean energy of the electrons is

$$\begin{aligned}\langle E\rangle &= \tfrac{1}{2}mv^2 \\ &= e\mathscr{E}\lambda(3\Gamma)^{-1/2}\end{aligned} \tag{10.11}$$

while the diffusion coefficient is given by

$$D = \left[\frac{2e\mathscr{E}\lambda^3}{9(3\Gamma)^{1/2}m}\right]^{1/2} \tag{10.12}$$

Note that the combination of terms

$$\begin{aligned}E_k &= \frac{eD\mathscr{E}}{w_\parallel} \\ &= \langle E\rangle\end{aligned} \tag{10.13}$$

gives a directly measurable indication of the characteristic energy of the electrons in the gas.

Examination of Eqs. 10.9 – 10.13 shows that they all vary monotonically with the mean free path for electrons in the gas. The dependence is strongest for the diffusion coefficient, which is proportional to $\lambda^{3/2}$. The components of the drift velocity also increase for increasing fractional energy loss per collision, while the mean energy and diffusion coefficient decrease.

Accurate calculations of the properties of mixtures of gases can be made using transport theory [4 – 6]. The theory uses density and energy conservation to obtain a set of equations for the distribution function $F(E)$ for a free electron in an external electric or magnetic field. Elastic and inelastic cross sections for electrons in the relevant gases are used as input. Once the equations have been solved for $F(E)$, the transport coefficients, such as w and D, can be obtained from appropriate integrals over the energy.

The optimum gas mixture for a wire chamber is strongly dependent on

the intended application [6]. Table 10.2 indicates gas mixtures that give various desired properties. Gases with high specific energy loss are used for efficient detection of charged particles and photons. A gas with low specific energy loss would be used if it was important to minimize multiple scattering. High drift velocity gases are used in high rate environments, while a lower drift velocity improves the spatial resolution obtainable with electronics of a given speed. Small diffusion is desirable for good spatial resolution. Chambers are typically operated in a region where the drift velocity is independent of $\mathscr{E}$ (saturation region). The choice of the actual drift velocity that is used is influenced by the available drift path, particle intensity, and speed of the recording electronics.

Argon is widely used as a drift chamber gas. The argon may be mixed with gases consisting of heavy organic molecules, such as carbon dioxide or isobutane. These gases, known as quenchers, have many degrees of freedom and can efficiently absorb energy from the gas [7]. As a result, the effective temperature of the electron is reduced, the drift velocity is increased, and the diffusion is decreased. Sometimes a small amount of a third gas, such as dimethoxymethane (DMM), is also added. A typical composition is 68% Ar/30% C_4H_{10}/2% DMM.

Figure 10.3 shows measured drift velocities for argon–propane mixtures as a function of the applied electric field [8]. The curves have been displaced by 10 μm/ns from each other for clarity. The dotted line associated with each curve corresponds to a velocity of 50 μm/ns. Note that certain gas proportions result in drift velocities which are independent of $\mathscr{E}$. This phenomenon is quite important in achieving linear space–time correlations, since it minimizes the change in drift velocity as the electrons approach the sense wire. The drift chamber gas should not attach electrons, or else the detection efficiency will depend on the drift distance.

Table 10.2. *Properties of gas mixtures*

Desired property	Gas components
High specific mass	Xe
Low specific mass	H_2, He
High drift velocity	CH_4, CF_4
Low drift velocity	CO_2, dimethylether, He-C_2H_6
Small diffusion	hydrocarbons, CO_2, dimethylether, NH_3
Small magnetic deflection angle	CO_2, CO_2-isoC_4H_{10}
Electron capture	O_2, H_2O, CF_3Br, Freons

Source: A. Peisert and F. Sauli, CERN Report 84-08, 1984.

Figure 10.3 Drift velocities of argon – propane gas mixture as a function of electric field. (After B. Jean-Marie, V. Lepeltier, and D. L'Hote, Nuc. Instr. Meth. 159: 213, 1979.)

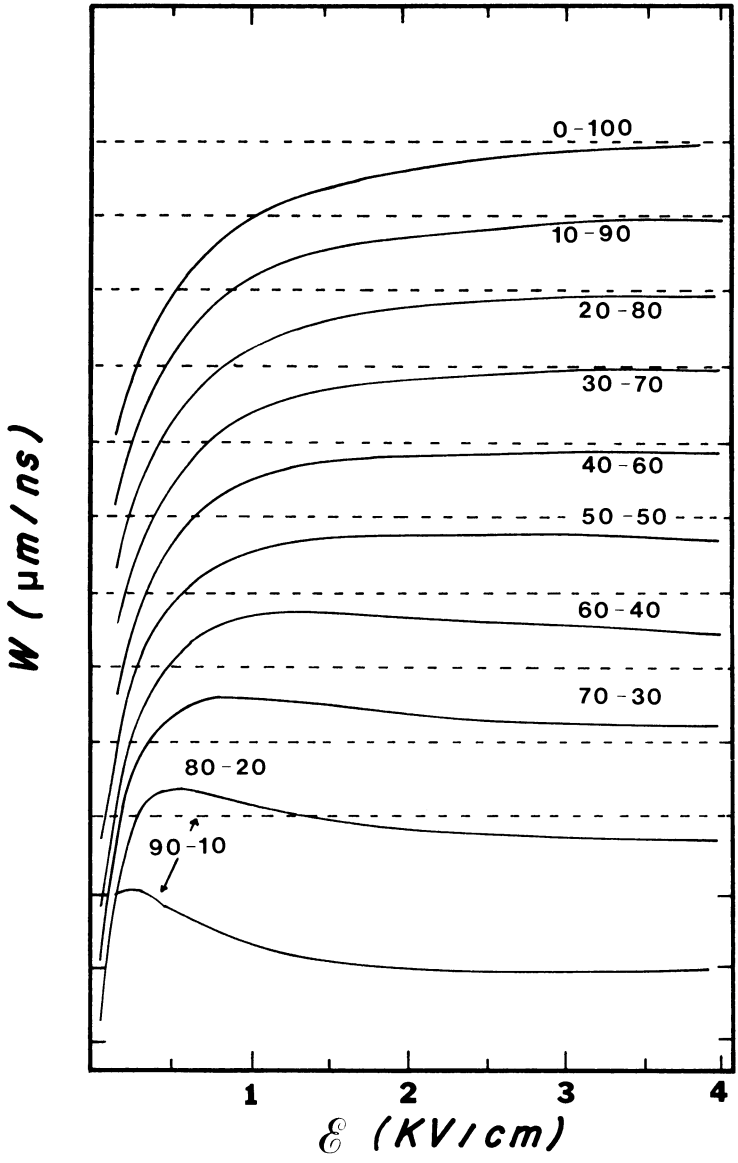

https://doi.org/10.1017/9781009290098.011 Published online by Cambridge University Press

10.2 Construction

Three major types of drift chambers are in common use: (1) planar chambers, (2) cylindrical chambers, and (3) proportional drift tubes. Cylindrical chambers are used to surround an interaction region, particularly at colliding beam machines. Proportional drift tubes are useful in large volume applications, such as for calorimeters. The choice of the size of the drift cell is influenced by the maximum expected event rate and track multiplicity. The maximum rate that can be tolerated per wire appears to be $\sim 10^4$ counts/mm-s [9].

Now let us consider several examples of actual chambers. The wire arrangement in the BNL MPS planar chambers with small 3.2 mm drift space is shown in Fig. 10.4. The drift space is bounded by planes of cathode wires held at a large negative potential [10]. The drifting electrons are collected on the grounded anode wires. Gold-plated tungsten wire 25 μm diameter is used for the anode, while 75-μm diameter stainless steel is used for the field and cathode wires. The electric field uniformity is improved by using field wires between the anodes. These wires are held at a slightly higher potential than the cathode.

The MPS chamber wires were strung on strong fiberglass–polyester frames and stacked together to form modules. The anode spacing of the x' measuring planes are displayed by half a drift cell width in order to help resolve the ambiguity of whether a track has passed to the right or left side of a given anode wire. Each module also contains y measuring planes and u and v ($\pm 30°$ to y) measuring planes. This enables each module to measure a vector on the particle's trajectory, which simplifies the pattern recognition. The chambers use a 79% Ar/15% C_4H_{10}/6% dimethoxymethane gas mixture. The maximum drift time for these chambers is 70 ns, and the space–time relation shown in Fig. 10.5 is quite linear. One nice feature of small drift spaces is that the $\mathscr{E} \times \mathbf{B}$ displacement is small.

It is usually desirable for the field to be uniform in the drift space, so that x varies linearly with t. In chambers with large drift spaces located in a

Figure 10.4 Wire arrangement for the MPS planar drift chambers. (A) anode wire, (F) field shaping wire, and (C) cathode wires. The anode–cathode spacing is 6.4 mm and the anode–field wire spacing is 3.2 mm.

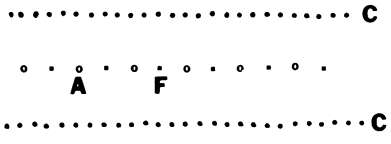

https://doi.org/10.1017/9781009290098.011 Published online by Cambridge University Press

magnetic field, the potential on each cathode wire may be gradually varied by applying the high voltage through a divider chain [1].

Cylindrical drift chambers have found wide acceptance at intersecting storage rings. Wagner [11] separates the chambers that have been built so far into "classical" and "pictorial" categories. The classical chambers are defined to have 15–20 planes of wires, approximately half of which are oriented parallel to the magnetic field axis. These planes are used for pattern recognition. The other wire planes are rotated by a small angle with respect to the field axis and are used to resolve ambiguities and to determine the z coordinates of the reconstructed tracks. In a pictorial drift chamber, on the other hand, 40–200 points are recorded for each track. The high measurement density is essential for good separation of closely spaced tracks and for finding secondary vertices and decays. The term *pictorial* arises since there are sufficient hits in the chamber to recognize tracks without fitting. Such chambers typically put a much larger burden on the readout electronics. The TPC, discussed in Section 4, is an example of this type of chamber. Table 10.3 lists characteristics of some large cylindrical drift chamber systems.

Figure 10.5 Drift time versus track position in the MPS planar drift chambers in a 10-kG field. (After E. Platner, Brookhaven National Laboratory report BNL 30898.)

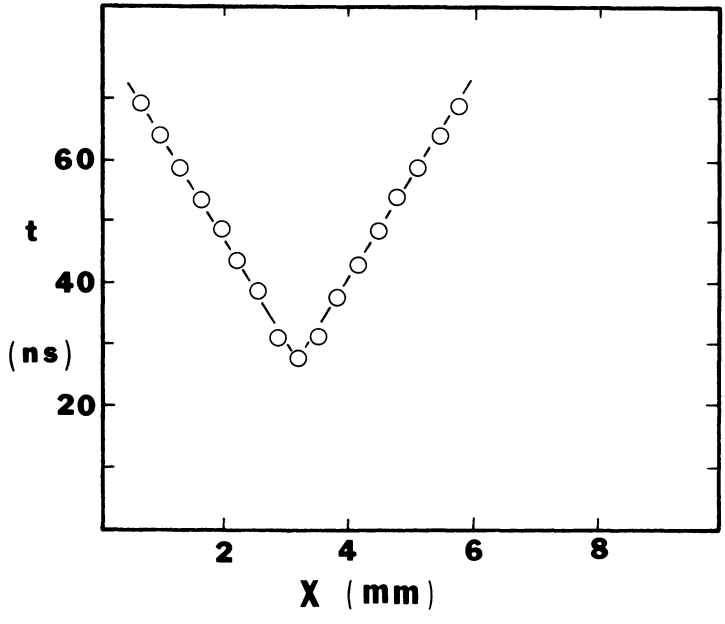

Table 10.3. *Representative cylindrical drift chamber systems*

Detector	Number of sense wires	Maximum wire length (cm)	Sense wire diameter (μm)	Field wire diameter (μm)	Gas mixture
UA-1	6110	220	35Ni-Cr	100Cu-Be	40 Ar/60 eth
AFS	3444	140	30SS-Ni	100Cu-Be	50 Ar/50 eth
HRS	2448	253	37W	125Be-Cu	89 Ar/10 CO
JADE	1536	240	20W-Re	100Be-Cu	89 Ar/8 CH_4
MARK II	3204	264	38Cu-Be	152Cu-Be	50 Ar/50 eth
TASSO	2340	352	30W	120Mo	90 Ar/10 CH
CELLO	~3000	220	20W-Re	50,100Cu-Be	90 Ar/10 CH

[a] Abbreviations: CD, charge division; HP, high pressure (4 atm).
Source: M. Barranco Luque et al., Nuc. Instr. Meth. 176: 175, 1980; O. Botner et al., Nuc
Chapman, D. Nitz, A. Seidl, and R. Thun, Nuc. Instr. Meth. 203: 119, 1982; W. Davies-Wh
H. Boerner et al., Nuc. Instr. Meth. 176: 151, 1980; W. deBoer et al., Nuc. Instr. Meth. 176:
156: 283, 1978.

The central detector of the TASSO spectrometer at PETRA ues a cylindrical drift chamber 2.56 m in diameter and 3.52 m in length inside a solenoidal magnetic field [12]. The chamber contains 2340 drift cells. The sense wires are 30-μm diameter gold-plated tungsten, while the cathode uses 120-μm gold-plated molybdenum. The sense wires were tensioned to 0.8 N and the cathode wires to 3 N. All the wires were stretched between two aluminum end plates, which were spaced apart by tubes on the inside and outside radii of the drift region. The chamber used a 90% Ar/10% CH_4 gas mixture.

Figure 10.6 Electric field lines in the TASSO drift cell (H. Boerner et al., Nuc. Instr. Meth. 176: 151, 1980.)

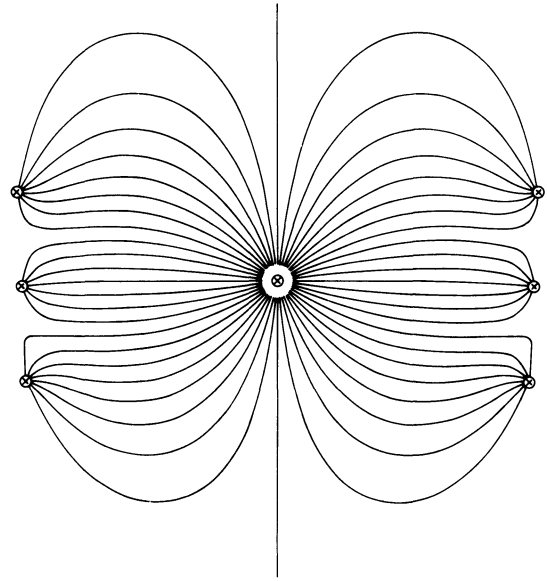

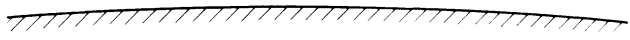

https://doi.org/10.1017/9781009290098.011 Published online by Cambridge University Press

The field shape in the 16-mm drift space is shown in Fig. 10.6. The high voltage distribution system contains both active and passive circuits to prevent any wire from drawing an excessive current. The high voltage efficiency curve had a plateau above 2400 V. The efficiency below the plateau is adversely affected by a magnetic field. For drift distances larger than about 6 mm the space–time relationship is strongly affected by the angle of the particle trajectory. This is largely caused by the deflection of the electron trajectories in the magnetic field. A typical event in the chamber is shown in Fig. 10.7.

Proportional drift tubes offer a number of advantages over wire chambers for certain applications, particularly those involving large solid angle coverage. They are easier to construct, cheaper, modular, and have a self-supporting structure [13]. A broken wire only eliminates a single cell instead of a whole plane. They have the disadvantages of poorer resolution, a nonuniform electric field, and an enhanced sensitivity to impurities in the gas.

Figure 10.7 A typical event in the TASSO cylindrical drift chamber (H. Boerner et al., Nuc. Instr. Meth. 176: 151, 1980.)

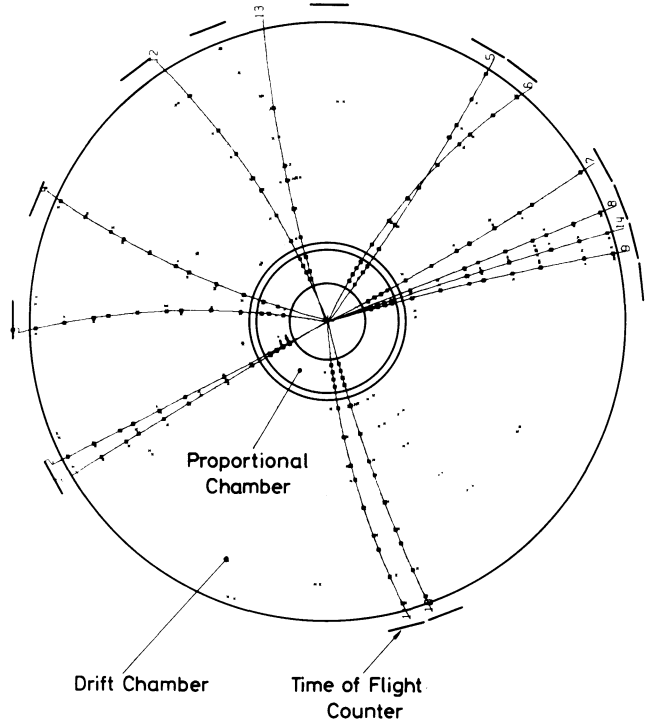

https://doi.org/10.1017/9781009290098.011 Published online by Cambridge University Press

The CHARM neutrino detector at CERN [14] contains a system of 12,600 proportional tubes. Figure 10.8 shows the details of the mechanical construction. The 50-μm stainless steel sense wires are mounted in a 29 mm $\times$ 29 mm $\times$ 4 m extruded aluminum tube. The wires are stretched to a tension of 1 N. The tubes contain a 95% Ar/5% C_3H_8 gas mixture. The gas amplification depends strongly on the high voltage, gas density, and gas composition. A gas control system was used to stabilize the pressure and thus reduce gain variations.

The European Muon Collaboration at CERN [13] have constructed a system containing 1100 PDTs. The tubes are circular with a 5-cm inner diameter and are up to 2 m in length. The tubes are constructed from 1-mm-thick bakelight paper. The cathode consists of a conductive paint on the inside of the tube. The anode is a 20-μm gold-plated tungsten wire. The tubes contained an 80% Ar/20% ethane gas mixture and had a spatial resolution of 0.18 mm.

Figure 10.8 Construction details of the CHARM proportional drift tubes. (1) sense wire, (2) aluminum tube, (3) wire support, (4) gas inlet/outlet, (5) insulator, (6) support and manifold, and (7) cover plate. (A. Diddens et al., Nuc. Instr. Meth. 176: 189, 1980.)

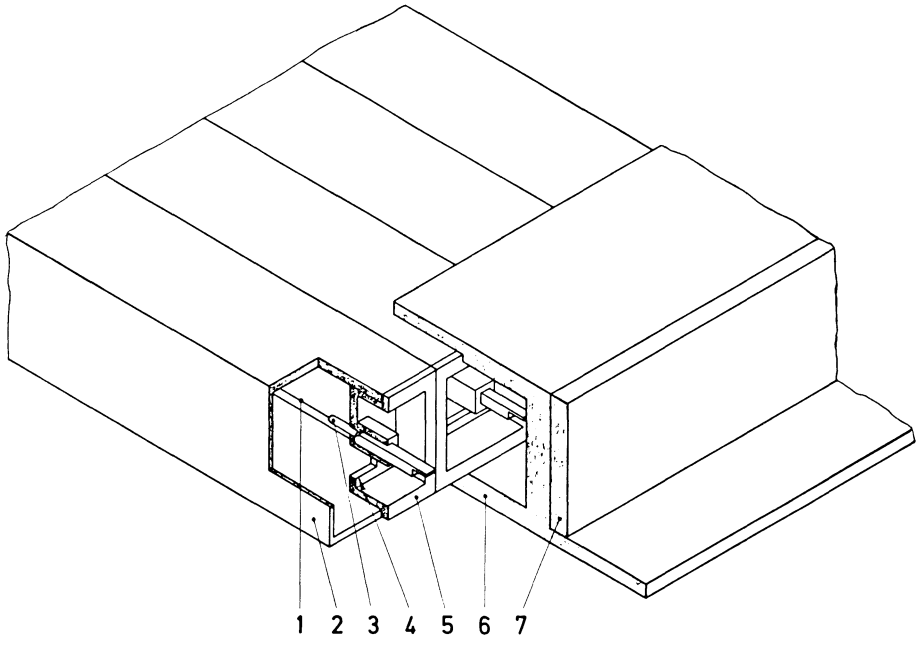

https://doi.org/10.1017/9781009290098.011 Published online by Cambridge University Press

10.3 Readout electronics

The minimum requirement for a drift chamber electronics is to specify which wire has detected a pulse and to measure the elapsed time between some reference signal t_0 and the time the pulse is collected by the sense wire. Figure 10.9 gives the fundamental components of a system to measure the drift time for a single wire. The reference time is usually provided by a scintillation counter upstream of the drift chambers. This signal can be used as a start signal to a TDC. The anode wire from the drift chamber gives the stop pulse.

A multiwire readout scheme contains a number of independent digitizing channels [1]. A start signal enables the first channel scaler to count oscillator pulses from a clock. This is stopped by a pulse from any of the anodes. The wire number of the active wire is then stored in a latch. The data acquisition electronics for detectors with large arrays of wires are generally designed to record data only from the active wires. Commercial preamplifier–discriminator integrated circuits and special purpose TDC

Figure 10.9 Simple readout system for drift chamber signals. (HV) high voltage, (A) preamplifier, (D) discriminator, (TDC) time to digital convertor, and (DA) data acquisition.

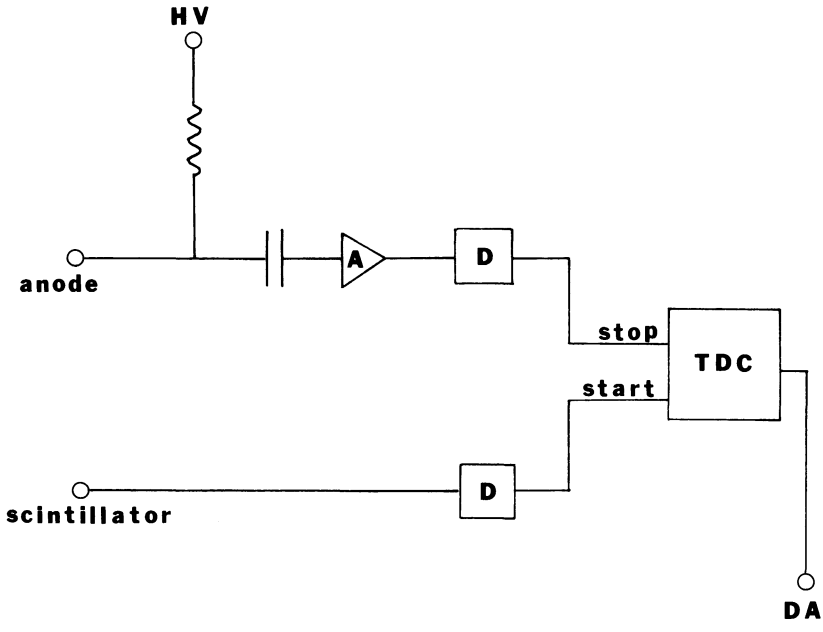

https://doi.org/10.1017/9781009290098.011 Published online by Cambridge University Press

and controllers are also available to make drift chamber signals available to CAMAC data systems.

A block diagram of the readout electronics for the CHARM PDTs [14] is shown in Fig. 10.10. The input signal from each sense wire is divided between the charge amplifier and the timing discriminator. Since the drift velocity in the argon – propane gas mixture is slow, the readout electronics can be built using TTL integrated circuits. The electronics could function as an 8-bit ADC or TDC. The maximum deadtime was less than 15 μs.

Pictorial drift chambers measure the drift time and signal charge using fast electronics capable of responding to more than one hit [11]. This can be done using an analog storage device, such as a CCD, which samples the input signal at a rate determined by an external clock. Another technique is to use flash ADCs, which sample the input signal with short ($\sim$32-ns) integration times.

Fast electronics are required to take full advantage of the intrinsic time resolution of drift chambers. A "time stretcher" circuit can be used to expand the time interval and then read it out with slower electronic circuits [1]. The readout system employed with the MPS planar chambers uses amplifiers with a 4-ns risetime [10]. The signal is shaped and fed into a discriminator – comparator. Here the reference voltage can be varied to change the signal threshold. A 256-bit shift register acts as a digital delay and time digitizer. The discriminator output is continuously fed into the

Figure 10.10 Readout system for CHARM proportional drift tubes. (A. Diddens et al., Nuc. Instr. Meth. 176: 189, 1980.)

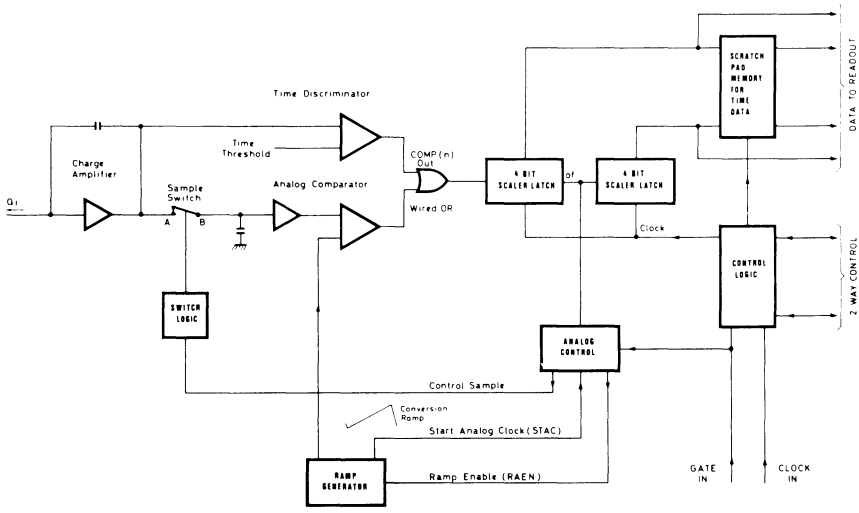

https://doi.org/10.1017/9781009290098.011 Published online by Cambridge University Press

shift register. An appropriately delayed trigger signal stops the register after about 1 μs. Active channels contain YES bits somewhere is the last 32 bits of the register. The position of the furthest YES bit provides a measure of the drift time to within 4 ns.

The analog signal methods listed in Table 9.4 have also been employed in drift chambers to measure a second coordinate of a particle's trajectory through the chamber. The European Muon Collaboration [13] used delay lines with their proportional drift tubes, shown in Fig. 10.8. The delay line assembly was mounted adjacent to the last plane of PDTs in each assembly in order to measure the position of the interaction along the wire. The positive signal on the resistive cathode induced a signal on the delay line electrodes. The delay line followed a folded zigzag path to the electronics at each end. The position resolution using the time information from both ends was 6.3 mm.

An auxiliary system of electronics may be necessary in large chamber arrays to monitor the performance of the chambers. For example, Daum et al. [15] have used a minicomputer to monitor the performance of their chambers at the CERN SPS. The minicomputer can be used between beam spills to check for electronic faults, inefficient modules, timing errors, and missing wires.

10.4 Performance

There are a number of important performance characteristics for drift chambers, including efficiency, double track resolution, and operation in a magnetic field. However, the most important property is usually the spatial resolution.

A large number of effects influence the ultimate spatial resolution that can be achieved [16]. First, there are limitations due to physical processes. We have seen that a charged particle passing through the gas in a drift cell leaves behind a trail of ions. There are about 30 electron–ion pairs created per centimeter in argon at STP. However, the actual number and size of these ion clusters and their distribution along the path of the particle is subject to statistical fluctuations. In addition, as the electrons begin to drift toward the anode under the influence of the electric field, the cloud will spread out due to diffusion, multiple scattering, and secondary ionization.

The spatial uncertainty arising from diffusion is [1]

$$\sigma^2 = 2\int_0^x \frac{D}{w}\,dx \tag{10.14}$$

https://doi.org/10.1017/9781009290098.011 Published online by Cambridge University Press

and thus one wants a gas with a small value for the ratio D/w. The diffusion coefficient is not isotropic. Fortunately, the coefficient $D_\parallel$ for diffusion along the direction of the electric field is much smaller than the coefficient $D_\perp$ for transverse diffusion. It is $D_\parallel$ that affects the arrival time of the electron cloud at the sense wire. Equation 10.7 can be written in terms of the characteristic energy as

$$\sigma_x^2 = 2E_k x/e\mathscr{E} \tag{10.15}$$

The addition of a multiatomic molecule like isobutane to pure argon increases the fractional energy loss per collision Γ because energy can then be absorbed into vibrational and rotational modes. According to Eqs. 10.11 and 10.13, this reduces E_k and thus the dispersion σ_x. The effect that this dispersion has on the actual spatial resolution depends on the detection method [7].

Another physical process is fluctuations in ion multiplication near the anode wire. These processes affect the arrival time of electrons at the anode.

A second set of limitations are due to inaccuracies in the chamber construction. The major contribution arises from errors in the wire positions. These may be random errors due to the tolerances in the support structure, or systematic errors such as gravitational sagging or electrostatic deflections.

Table 10.4. *High resolution drift chambers*

Chamber	Principle
Scintillating drift chamber	detects secondary gas scintillation near anode with PMT; fast response; no space charge distortion
Time projection chamber; jet chamber; imaging chamber	track segments continuously sampled and recorded electronically; large volume
Microjet chamber	thin anode wires
Precision drift imager	only accepts small segments of ionization trail; good two-track separation
Time expansion chamber	low velocity drift region; flash ADC readout
Parallel plate avalanche chamber	uniform electric field in gain region
Multistep avalanche chamber	amplifying regions separated by wire grids; single electron imaging

Source: G. Charpak and F. Sauli, Ann. Rev. Nuc. Part. Sci. 34: 285, 1984.

A third set of limitations are due to the electronics. There will be uncertainties in the time of arrival of the scintillator reference pulse and anode signal due to jitter and slewing in the discriminator thresholds. High frequency noise may be present on the chamber signal. In addition, the drift time cannot be measured more accurately than the size of the time bins in the timing circuitry. The electronics should be designed so that these errors do not limit the chamber's performance.

Finally there are limitations in converting the time interval into a spatial distance. There may be uncertainties in the drift velocity due to variations in the electric field, the magnetic field, and the pressure, temperature, and composition of the chamber gas. Table 10.4 lists a number of drift chambers specially constructed to obtain high resolution (10–50 μm). These devices frequently use high pressure gas, which improves the spatial localization by increasing the primary ionization and decreasing diffusion.

The resolution of one in a series of chambers can be determined by fitting a track through all the chambers but one and then measuring the deviation of the measured position in that chamber from the fitted value. Figure 10.11 shows a set of measurements of spatial accuracy obtained this way as a function of the distance of the particle from the sense wire.

Figure 10.11 Contributions to drift chamber spatial resolution. (F. Sauli, CERN report 77-09.)

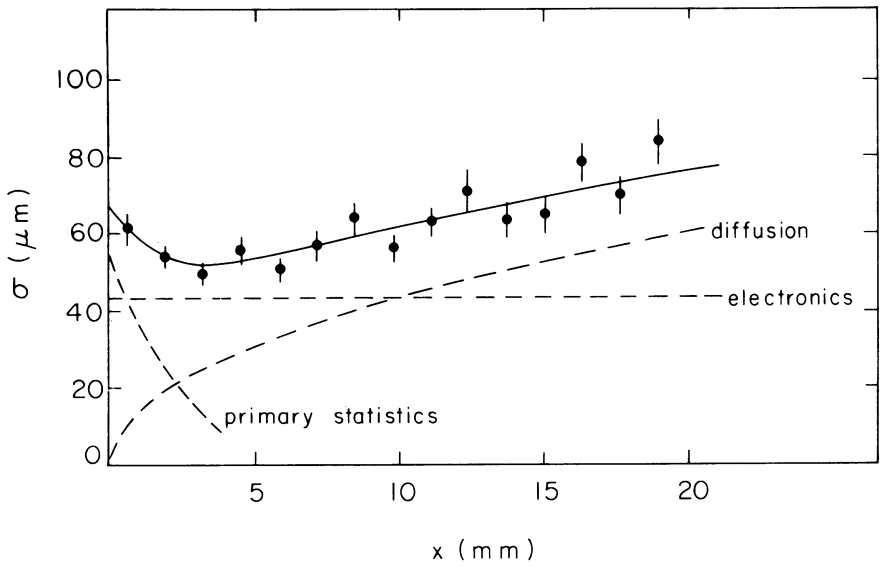

https://doi.org/10.1017/9781009290098.011 Published online by Cambridge University Press

Also shown are the contributions to the resolution arising from primary ion statistics, electronics, and diffusion. Fluctuations in the primary ionization are chiefly important near the sense wire. The electronics contribution is independent of distance, while the time spread from diffusion increases with distance.

The space–time relation $x(t)$ can be determined by measuring the time spectrum of a uniformly distributed beam since [2]

$$\frac{dN}{dt} = \frac{dN}{ds}\frac{ds}{dt} = kw(t) \tag{10.16}$$

where k is constant. Thus, the time distribution gives a measure of $w(t)$, and by Eq. 10.1 the integral of the distribution gives the space–time relation.

Wire chambers suffer a degradation in performance after prolonged exposure to radiation. Turala and Vermeulen [17] observed a significant drop in drift chamber efficiency when the accumulated number of charges collected on the anode wires reached 10^{17} cm^{-1}. The loss of efficiency was nonuniform and nonsymmetrical. Whitish-gray deposits were found on the irradiated anode wires. The deposits are believed to contain silicon and hydrocarbon fragments. They could be removed by cleaning the wires with acetone.

10.5 Particle identification

A number of wire chambers have been built that combine the functions of measuring particle coordinates with identifying the type of particle that made the track [18]. The particle identification is achieved by making measurements of dE/dx in the drift chamber gas. In the region of the relativistic rise the expected energy loss differs slightly depending on the mass of the particle. The design goal for any dE/dx detector is to maximize the separation D in the relativistic rise for the particles of interest, at the same time obtaining the best possible resolution σ in the measurement of dE/dx. The usual figure of merit, or resolving power, is D/σ.

Measurements of dE/dx in the gas of a wire chamber are very difficult because of the small difference expected between different mass particles, the saturation of the effect at large $\beta\gamma$ or gas density, and the large fluctuations in energy loss for a given gas sample. The energy loss in a thin absorber follows a Landau-like distribution, which as we have seen is characterized by a long high energy loss tail. The width of this distribution

is much broader than the size of the relativistic rise difference. The size of the fluctuations can be reduced by increasing the gas sample thickness up to a point, after which the width of the distribution is constant at about 30% FWHM. The sample thickness may be increased by either increasing the gas thickness or by operating the chamber at higher pressure. However, while higher pressure improves the single measurement resolution, it decreases the size of the relativistic rise effect.

The usual method is to sample the ionization loss many times. This can be done by providing many planes of transverse drift regions or by using a longitudinal drift geometry, where the electric field is approximately parallel to the particle's trajectory. When many energy loss samples are taken, the mean energy loss can be calculated using the truncated mean technique. The largest 40% or so of the energy loss measurements are discarded before calculating the mean. This method gives better resolution than averaging all the data.

A number of systematic effects must also be understood before the energy loss resolution can be reduced below the 10% level [18]. The response can depend on track position since (1) different wires may be involved, (2) there may be a variation in gas gain along the length of the wire, (3) the amount of collected charge depends on the initial distance of the incident particle from a given anode wire, (4) electrons are more likely to be attached by impurities such as O_2 in the gas the further the incident particle was from the anode wire, and (5) saturation of gas gain for tracks with a small angle with respect to the anode wires. The response of the chamber depends on the incident particle conditions since, first, the incident rate affects the space charge from the buildup of positive ions and reduces the gas gain and, second, there can be an overlap in the signals of two closely spaced tracks. Other systematic effects include cross talk between neighboring cells and baseline shifts.

Table 10.5 shows some gas properties that are important for designing a dE/dx detector [19]. The resolution in measuring dE/dx in a gas is given by the percentage FWHM. For a single measurement this is $\sim 30-60\%$. The resolution from taking the truncated mean of 64 independent measurements is much smaller, typically $5-11\%$. Note that the resolution improves with increasing pressure and that the pure hydrocarbons have better resolution than the noble gas mixtures. The next column, labeled relativistic rise, gives the ratio of the truncated mean energy losses for electrons and protons. The largest effect is observed in the xenon gas mixture. Unlike the resolution, the relativistic rise effect decreases at

Table 10.5. *Gas mixtures for dE/dx measurements*

Gas mixture	P (atm)	$\mathscr{E}/P$ (kV/cm-atm)	FWHM Single sample	FWHM T
90% Ne + 10% C_2H_6	1.0	0.31	57	
	2.0	0.32	47	
95% Ar + 5% CH_4	1.0	0.18	59	1
96.4% Xe + 3.6% C_3H_8	0.9	0.40	62	
CH_4	1.0	0.31	45	
C_2H_4	1.0	0.34	41	
C_2H_6	1.0	0.36	38	
	2.0	0.37	31	
	3.0	0.31	29	
C_3H_8	1.0	0.36	34	

Source: I. Lehraus, R. Matthewson, and W. Tejessy, Nuc. Instr. Meth

https://doi.org/10.1017/9781009290098.011 Published online by Cambridge University Press

increasing pressure. The last two columns give the resolving powers for $e-\pi$ and $\pi-p$ separation. The noble gas mixtures clearly give the best performance.

In the longitudinal drift geometry technique the particles pass through the chamber parallel to the drift field. Special readout electronics are then used to sample the charge collected over short time intervals. Maximum resolution should be obtained using a gas with small drift velocity and small diffusion coefficient, so that the arriving ionization clusters are well separated. For example, Imanishi et al. [20] have used this technique to make dE/dx measurements in a drift chamber with a 51-mm drift space filled with 90% Ar/10% CH_4. The pulse heights were measured using flash ADCs with a 40-ns sampling time. The time-sliced pulse height spectrum showed a broad plateau over a region of 1.4 μs, which corresponds to the gas sampling thickness. The long time-constant tail in the current pulse was filtered out to prevent pileup. The truncated mean method was used to calculate the most probable energy loss. The resolving power was independent of the fraction of samples retained over the range 50–80%.

Some dE/dx detectors rely on counting the number of ionization clusters instead of measuring the total amount of liberated charge [18]. This method reduces the large fluctuations in single measurements, since the number of clusters that are created follows a Poisson distribution instead of a Landau-like one. The mean number of clusters is given by

$$\bar{n} = \frac{\alpha t}{\beta^2} \frac{a}{E_{\text{ion}}} \left(\ln \frac{2mc^2}{E_{\text{ion}}} + 2 \ln \beta\gamma - \beta^2 + b \right) \tag{10.17}$$

where E_{ion} is the ionization energy, $a \sim 0.3$ and $b \sim 3$ are gas dependent shell corrections, and

$$\alpha t = 0.153(Z/A\rho t)$$

where αt is in MeV when ρt is in g/cm^2. The mean number of clusters varies from 5 to 45 for different gases at atmospheric pressure. A second advantage of the method is that the information is inherently digital, so that systematic errors should be smaller. One problem with cluster counting is that the smallest cluster, involving a single electron, must be detected with high efficiency since such clusters are the most common. Another disadvantage is that the relativistic rise in the number of clusters reaches its plateau value faster than the rise in energy loss.

A time projection chamber (TPC) is a drift chamber that provides spatial information in three dimensions, as well as measurements of dE/dx for particle identification [21–23]. The essential feature of a TPC is that the electric field in the chamber is parallel to the magnetic field

from a spectrometer magnet. This arrangement reduces the diffusion of electrons in the gas because the magnetic field forces the drifting electron to wind around the electric field lines. As a consequence, the electron can drift over a long distance and still provide good spatial resolution. The detector has a large solid angle acceptance and can simultaneously measure a large number of tracks.

The first such chamber was designed for use around an intersection point at the PEP colliding beam facility at SLAC [23]. An 80% Ar/20% CH_4 gas mixture is used to provide high mobility and low electron attachment. After the passage of an ionizing particle the liberated electrons cross a large ($\sim$1-m) drift space in the direction of the sense wire plane, as shown in Fig. 10.12. It was necessary to carefully shape the electrostatic drift field in order to eliminate track distortions. Grounded grid wires focus the electrons toward the sense wires and collect stray positive ions. Field wires located between the sense wires reduce cross talk among neighboring sense wires due to the motion of positive ions.

The trajectory of the particle can be reconstructed using the distribution of sense wire hits, the drift times to the sense wires, and the charge distribution on cathode pads beneath some of the sense wires. These 7.5-mm-wide strips run parallel to the sense wires and are subdivided into a number of individual parts, each with its own readout. The spatial

Figure 10.12 Principle of TPC readout. (Courtesy of University of California, Lawrence Berkeley Laboratory.)

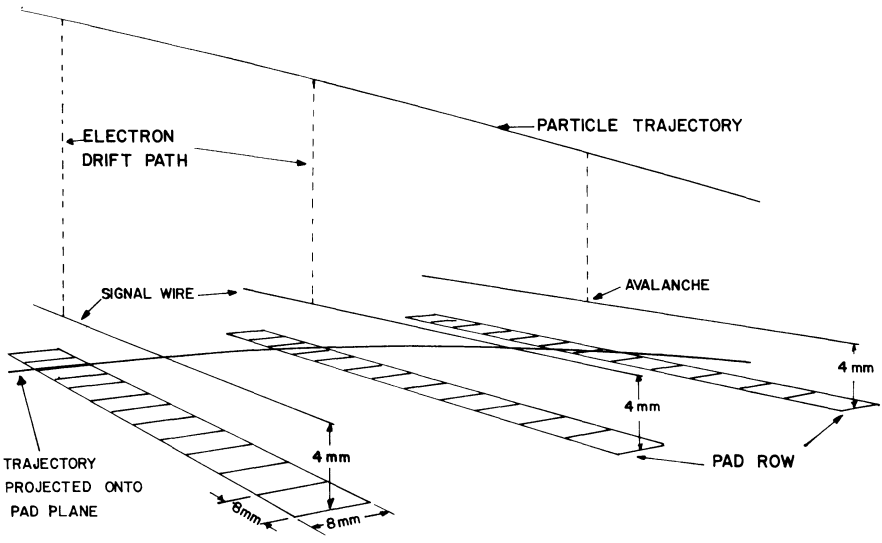

https://doi.org/10.1017/9781009290098.011 Published online by Cambridge University Press

resolution of the chamber was 160 μm in the radial direction and 350 μm along the axis.

The particle identification is achieved by measurements of energy loss. The magnitude of the signal on each sense wire and cathode pad is sampled in $\lesssim$100-ns time intervals using a linear charge coupled device. The chamber is operated at a pressure of 8.5 atm to provide sufficient path length in the gas. Good resolution ($\sim$3% rms) on the determination of the energy loss can be obtained by taking the truncated mean of many independent measurements.

References

A good introduction to drift chambers can be found in references 1 and 2. The latest developments for all aspects of drift chamber technology can be found in the proceedings of Wire Chamber Conferences given in reference 3.

[1] P. Rice-Evans, *Spark, Streamer, Proportional, and Drift Chambers,* London: Richelieu, 1974, Chap. 10.

[2] F. Sauli, Principles of operation of multiwire proportional and drift chambers, CERN Report 77-09, 1977.

[3] Nuc. Instr. Meth. 176: 1–432, 1980; Nuc. Instr. Meth. 217: 1–381, 1983.

[4] V. Palladino and B. Sadoulet, Application of classical theory of electrons in gases to drift proportional chambers, Nuc. Instr. Meth. 128: 323–35, 1975.

[5] J. Townsend, *Electrons in Gases,* London: Hutchinson, 1947.

[6] A. Peisert and F. Sauli, Drift and diffusion of electrons in gases: A compilation (with an introduction to the use of computing programs), CERN Report 84-08, 1984. This reference contains measurements of drift velocities and diffusion coefficients for a large variety of gas mixtures.

[7] B. Sadoulet, Fundamental processes in drift chambers, Physica Scripta 23: 434–45, 1981.

[8] B. Jean-Marie, V. Lepeltier, and D. L'Hote, Systematic measurement of electron drift velocity and study of some properties of four gas mixtures: A-CH_4, A-C_2H_4, A-C_2H_6, A-C_3H_8, Nuc. Instr. Meth. 159: 213–9, 1979.

[9] G. Charpak, Multiwire and drift proportional chambers, Phys. Today, Oct. 1978, pp. 23–30.

[10] S. Eiseman, A. Etkin, K. Foley, R. Longacre, W. Love, T. Morris, S. Ozaki, E. Platner, V. Polychronakos, A. Saulys, C. Wheeler, S. Lindenbaum, M. Kramer, and Y. Teramoto, The MPS II drift chamber system, IEEE Trans. Nuc. Sci. NS-30: 149–52, 1983.

[11] A. Wagner, Central detectors, Physica Scripta 23: 446–58, 1981.

[12] H. Boerner, H. Fischer, H. Hartmann, B. Lohr, M. Wollstadt, D. Cassel, U. Kotz, H. Kowalski, B. Wiik, R. Fohrmann, and P. Schmuser, The large cylindrical drift chamber of TASSO, Nuc. Instr. Meth. 176: 151–7, 1980.

[13] C. Broll, A. Charveys, Y. DeClais, J. Favier, M. Lebeau, M. Moynot, and G. Perrot, Large drift tube arrays with external delay line readout, Nuc. Instr. Meth. 206: 385–95, 1983.

[14] A. Diddens, M. Jonker, J. Panman, F. Udo, J. Allaby, U. Amaldi, G. Barbiellini, A. Baroncelli, V. Blobel, G. Cocconi, W. Flegel, W. Kozanecki, E. Longo, K. Mess, M. Metcalf, J. Meyer, R. Orr, W. Schmidt-Parzefall, F. Schneider, A. Wetherell, K. Winter, F. Busser, P. Gall, H. Grote, P. Heine, B. Kroger, F. Niebergall, K. Ranitzsch, P. Stahelin, V. Gemanov, E. Grigoriev, V. Kaftanov, V. Khovansky, A.

Rosanov, R. Biancastelli, B. Borgia, C. Bosio, A. Capone, F. Ferroni, P. Monacelli, F. de Notaristefani, P. Pistilli, C. Santoni, and V. Valente, Performance of a large system of proportional drift tubes for a fine grain calorimeter, Nuc. Instr. Meth. 176: 189–93, 1980.

[15] C. Daum, L. Hertzberger, W. Hoogland, R. Jongerius, J. Knapik, W. Spierenburg, and L. Wiggers, Some features of a system of drift chambers for experiment NA11 at the SPS, Nuc. Instr. Meth. 176: 119–27, 1980.

[16] F. Sauli, Limiting accuracies in MWPC and drift chambers, Nuc. Instr. Meth. 156: 147–57, 1978.

[17] M. Turala and J. Vermeulen, Ageing effects in drift chambers. Nuc. Instr. Meth. 205: 141–4, 1983.

[18] A. Walenta, Performance and development of dE/dx counters, Physica Scripta 23: 354–70, 1981.

[19] I. Lehraus, R. Matthewson, and W. Tejessy, dE/dx measurements in Ne, Ar, Kr, Xe, and pure hydrocarbons, Nuc. Instr. Meth. 200: 199–210, 1982.

[20] A. Imanishi, T. Ishii, T. Ohshima, H. Okuno, K. Shiino, F. Naito, and T. Matsuda, Particle identification by means of fine samplng dE/dx measurements, Nuc. Instr. Meth. 207: 357–64, 1983.

[21] J. Macdonald (ed.), *The Time Projection Chamber,* American Institute of Physics Conf. Proc. No. 108, New York: AIP, 1984.

[22] R. Madaras and P. Oddone, Time projection chambers, Phys. Today, Aug. 1984, pp. 36–47.

[23] D. Fancher, H. Hilke, S. Loken, P. Martin, J. Marx, D. Nygren, P. Robrish, G. Shapiro, M. Urban, W. Wenzel, W. Gorn, and J. Layter, Performance of a time projection chamber, Nuc. Instr. Meth. 161: 383–90, 1979; J. Marx and D. Nygren, The time projection chamber, Phys. Today, Oct. 1978, pp. 46–53.

Exercises

1. Estimate the mean free path of electrons in an atmospheric drift chamber with a 2000-V/cm electric field. Use a typical drift velocity and assume that the random velocity of the electrons is $\sim 10^7$ cm/sec. What is the corresponding coefficient of diffusion?

2. Estimate the mean number of ion clusters left by a 50-GeV/c proton in a 2-mm argon drift chamber cell at a pressure of 2 atm. What is the FWHM of the cluster distribution?

3. What is the mean ionization energy loss for exercise 2? What is the FWHM of the energy loss distribution assuming a Landau distribution?

4. A drift chamber uses methane gas in a 2-kV/cm electric field. If the cell size is 1 cm, what should the least count of the readout electronics be, so that it is smaller than the time spread arising from diffusion?

5. Prove Eq. 4 in Appendix F.